Surface effects on spinodal decomposition in binary mixtures: The case with long-ranged surface fields

Sanjay Puri,[1,2] Kurt Binder,[1] and Harry L. Frisch[1,3]
[1]*Institut fur Physik, Johannes Gutenberg Universität Mainz, D-55099 Mainz, Germany*
[2]*School of Physical Sciences, Jawaharlal Nehru University, New Delhi 110 067, India*
[3]*Department of Chemistry, State University of New York at Albany, 1400 Washington Avenue, Albany, New York 12222*
(Received 9 May 1997)

We present detailed numerical results for phase-separation kinetics of critical binary mixtures in the vicinity of a surface that exerts a long-ranged attractive force on one of the components of the mixture. We consider surface potentials of the form $V(Z)\sim Z^{-n}$, where Z is the distance from the surface and $n=1,2,3$. In particular, we investigate the interplay of the surface wetting layer with the dynamics of domain growth. We find that the wetting layer at the surface exhibits power-law growth with an exponent that depends on n, in contrast to the case with a short-ranged surface potential, where the growth is presumably logarithmic. From correlation functions, we identify characteristic length scales in directions parallel and perpendicular to the surface. We observe a regime of accelerated growth in the parallel direction and critically examine some possible explanations for this. [S1063-651X(97)02212-5]

PACS number(s): 68.10.−m, 68.45.Gd, 64.75.+g

I. INTRODUCTION

There has been much experimental and theoretical interest in the phase separation kinetics of binary (AB) mixtures in the presence of a surface with a preferential attraction for one of the components of the mixture [1–3]. Typically, the surface is completely or partially wetted by the preferred component and becomes the origin of anisotropic spinodal decomposition waves, which propagate into the bulk perpendicular to the surface. This phenomenon has been referred to as ''surface-directed spinodal decomposition'' [4]. The morphology of these waves depends critically on the relative strengths of the surface field, the AB interfacial tension, and thermal noise, which determine whether the surface is completely or partially wetted by the preferred component.

In recent work we formulated a phenomenological model [5,6] for surface-directed spinodal decomposition in the presence of surfaces that exert a short-ranged (δ-function) potential on the preferred component. Our modeling was based on a master-equation formulation of an appropriate microscopic model, viz., the semi-infinite Ising model with Kawasaki spin-exchange kinetics. We have used this phenomenological model to obtain extensive numerical results [6] for this problem in the limit where the surface field leads to a complete wetting of the surface by the preferred component. Our results can be briefly summarized as follows. First, our model was able to replicate the experimentally observed morphology [4] of surface-directed spinodal decomposition waves. Second, we found that the growth of the wetting layer did not appreciably interfere with domain growth because of the extremely slow kinetics of wetting. Nevertheless, there was a marked anisotropy of coarsening domains in the vicinity of the surface. These domains were characterized by time-dependent length scales perpendicular and parallel to the surface, which we refer to as $L_{\perp}(\tau)$ and $L_{\parallel}(\tau)$, respectively, where τ is the time. We observed that both $L_{\perp}(\tau)$ and $L_{\parallel}(\tau)$ obeyed the Lifshitz-Slyozov (LS) growth law $L(\tau)\sim\tau^{1/3}$, though $L_{\perp}(\tau)<L_{\parallel}(\tau)$ because of the preferred orientational direction due to the layered structure at the surface.

In our earlier work, we cautioned that the case with a δ-function surface potential is experimentally somewhat unrealistic because surfaces generally exert long-ranged power-law potentials. In this paper, we extend our previous work to investigate the kinetics of phase separation near surfaces that exert long-ranged forces on the preferred component. Again, we focus on the case of ''strong'' surface fields [1], where the surface is completely wetted by the preferred component in equilibrium.

The problem of surface-directed spinodal decomposition has also been investigated numerically by a number of other authors [7–9] for cases with both short-ranged and long-ranged surface fields. These studies focus on the opposite limit from ours, viz., the surface field is weak compared to thermal noise and the interfacial tension, so that the surface is only partially wetted by the preferred component. In this situation, a strong universality characterizes domain growth and results for this limit are summarized in Ref. [1]. The results we present here are complementary to those in Refs. [7–9].

This paper is organized as follows. In Sec. II, we describe our model. Section III presents details of our numerical simulations and results therefrom. We end this paper with a summary and discussion of our results in Sec. IV.

II. DETAILS OF MODELING

In our earlier study of surface-directed spinodal decomposition with short-ranged surface forces [6], the appropriate phenomenological model consisted of the Cahn-Hilliard (CH) equation, which is widely used to model phase separation in the bulk [3], supplemented by two boundary conditions at the surface. The surface field only appeared in our model through the boundary conditions because of its short-ranged nature.

In the present study, we consider a surface located at

$Z=0$, which exerts a long-ranged (power-law) potential on the preferred component of the mixture, i.e.,

$$V(Z)=\begin{cases} -h_1, & Z<1 \\ -\dfrac{h_1}{Z^n}, & Z\geqslant 1, \end{cases} \tag{1}$$

where h_1 measures the strength of the potential and n specifies its range. The potential is set to be constant for $Z<1$ so as to control the divergence of the power-law form at $Z=0$. We arbitrarily consider the potential to be nondifferentiable at $Z=1$ (in dimensionless units [6]). Clearly, the precise location of the point of nondifferentiability is irrelevant because all length scales diverge with time. Then our phenomenological model for surface-directed spinodal decomposition with the surface potential $V(Z)$ as in Eq. (1) has the form (in dimensionless units [6])

$$\frac{\partial\phi(\vec{R},Z,\tau)}{\partial\tau}=-\nabla^2\Big[\phi(\vec{R},Z,\tau)-\phi(\vec{R},Z,\tau)^3 +\frac{1}{2}\nabla^2\phi(\vec{R},Z,\tau)-V(Z)\Big], \tag{2}$$

in conjunction with the boundary conditions

$$\frac{\partial\phi(\vec{R},0,\tau)}{\partial\tau}=h_1+g\,\phi(\vec{R},0,\tau)+\gamma\frac{\partial\phi(\vec{R},Z,\tau)}{\partial Z}\bigg|_{Z=0}, \tag{3}$$

$$0=\frac{\partial}{\partial Z}\Big[\phi(\vec{R},Z,\tau)-\phi(\vec{R},Z,\tau)^3 +\frac{1}{2}\nabla^2\phi(\vec{R},Z,\tau)-V(Z)\Big]\bigg|_{Z=0}. \tag{4}$$

In Eqs. (2)–(4), $\phi(\vec{R},Z,\tau)$ is the rescaled order parameter as a function of dimensionless space $(\vec{R},Z)$ and time τ [6]. The coordinate Z measures the distance from the surface and the coordinates $\vec{R}$ lie in the plane parallel to the surface. Equation (2) is the usual CH equation for phase separation in the bulk, with an additional term in the chemical potential due to the surface potential $V(Z)$. The boundary condition in Eq. (3) rapidly drives the order parameter at the surface to its equilibrium value and is identical to that for the short-ranged case [6]. The phenomenological parameters g and γ in Eq. (3) are related to the bulk correlation length, as explained in Ref. [6]. Finally, the boundary condition in Eq. (4) is the usual no-flux condition, which enforces conservation of the order parameter at the surface.

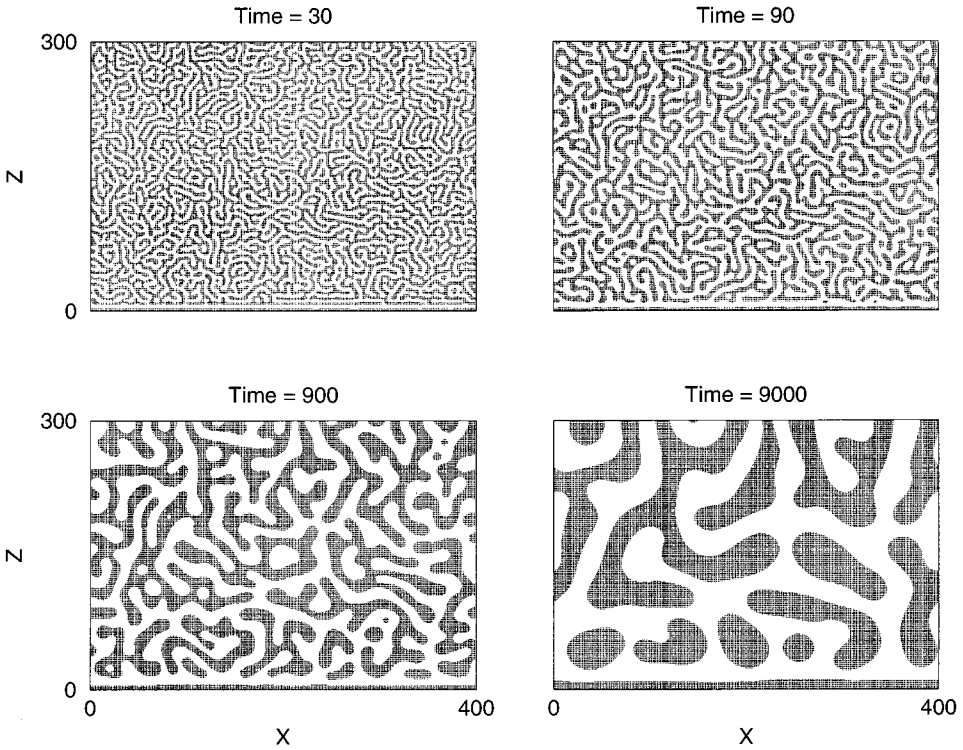

FIG. 1. Evolution pictures from a two-dimensional Euler-discretized version of our model in Eqs. (2)–(4) for spinodal decomposition in the presence of surfaces that exert a long-ranged attractive force on one of the components of a binary mixture. The lattice size was $N_X\times N_Z$ ($N_X=400, N_Z=300$) and the discretization mesh sizes were $\Delta\tau=0.03$ and $\Delta X=1.0$. The surface is located at $Z=0$ and was modeled by the boundary conditions in Eqs. (3) and (4). Flat boundary conditions were applied at the other end in the Z direction and periodic boundary conditions were applied in the X direction. The parameter values were $h_1=8$, $g=-4$, and $\gamma=4$ and the potential was specified by $n=3$, corresponding to nonretarded van der Waals interactions. The static equilibrium for these parameter values corresponds to complete wetting of the surface. The initial condition for this evolution consisted of uniformly distributed small-amplitude random fluctuations about a zero background, i.e., a critical quench. Regions with positive order parameter $\phi>0$ (say, A rich) are marked in black, whereas those with negative order parameter $\phi<0$ (say, B rich) are not marked. The dimensionless evolution times are specified above each frame.

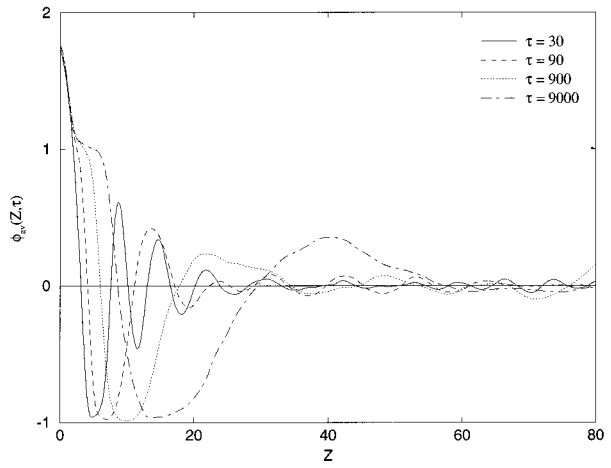

FIG. 2. Laterally averaged order parameter profiles $\phi_{\rm av}(Z,\tau)$ vs Z for the evolution depicted in Fig. 1. These were obtained by averaging the order parameter function in the X direction for a typical run and then averaging over 200 independent runs. From this picture, one can verify that the system evolves towards complete wetting of the surface: note the two-step relaxation of the order parameter profile. The decay starts from a surface value considerably larger than the bulk order parameter value (which is $\phi=1$ in our dimensionless units). The profile then stays at the bulk value of $\phi\simeq 1$ over some distance and finally decays from $\phi\simeq 1$ to $\phi\simeq -1$, corresponding to the interfacial profile between coexisting A-rich and B-rich phases.

The bulk CH equation has proven analytically intractable as yet because of its strong nonlinearity, in conjunction with the constraint of order-parameter conservation. Therefore, studies of bulk phase separation in the asymptotic regime have relied upon numerical simulations of this equation or equivalent coarse-grained models [10]. The introduction of a surface makes the problem considerably more complicated and we will again rely on numerical simulations of Eqs. (2)–(4) to obtain late-stage results.

III. NUMERICAL RESULTS

We have simulated Euler-discretized versions of Eqs. (2)–(4) on two-dimensional lattices of size $N_X\times N_Z$, with $N_X=400$ and $N_Z=300$. The surface was located at $Z=0$ and is modeled by the boundary conditions in Eqs. (3) and (4). Flat boundary conditions were applied at the other end in the Z direction and periodic boundary conditions were applied in the X direction. In this fashion, we attempt to model semi-infinite systems, with one free surface at $Z=0$, while bulk behavior is approached for large Z. The discretization mesh sizes used were $\Delta\tau=0.03$ and $\Delta X=1.0$, which were somewhat finer than those used in our earlier studies, i.e., $\Delta\tau=0.05$ and $\Delta X=1.5$ [6].

The initial conditions for each run consisted of the field ϕ being uniformly distributed with small-amplitude fluctuations about a zero background, mimicking the homogeneous system before the quench. We only consider the case of ''critical quenches,'' i.e., a symmetric binary mixture at critical concentration. All statistical quantities presented here were obtained as averages over 200 independent runs.

The fixed parameter values in our simulations were $g=-4$ and $\gamma=4$. (See Ref. [6] for a discussion that motivates this choice.) We used the long-ranged potential $V(Z)$ in Eq. (1) with field strengths $h_1=2$, 8, and 12 and exponents $n=1$, 2, and 3. The potential with $n=3$ corresponds to the usual case of (nonretarded) van der Waals interactions between the surface and the preferred component. The cases $n=1,2$ are not common, but could possibly be engineered in appropriate experimental situations. In the results presented subsequently, we will specify only the values of h_1 and n, as

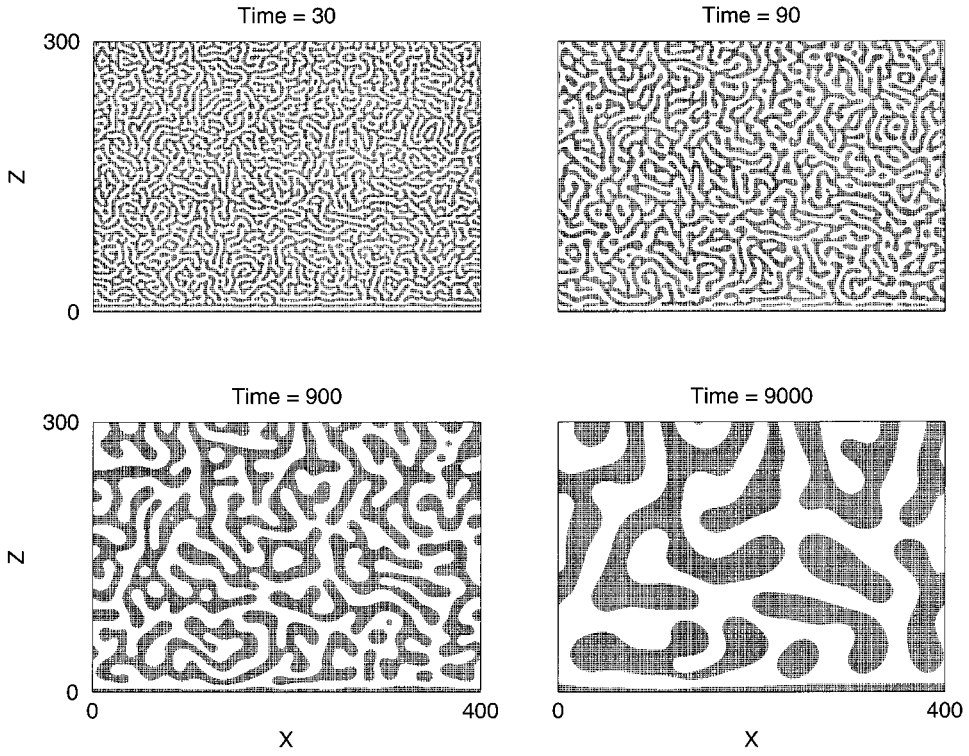

FIG. 3. Analogous to Fig. 1, but for parameter values $h_1=8$ and $n=\infty$ (corresponding to a δ-function surface potential). These parameter values also correspond to a completely wet static equilibrium.

g and γ were not varied in our simulations.

Figure 1 shows the temporal evolution of a disordered initial condition for the case $h_1=8$ and $n=3$, which corresponds to an equilibrium situation in which the surface is completely wetted by the preferred component. In the frames of Fig. 1, regions with a positive order parameter (say, A rich) are marked in black and those with a negative order parameter (say, B rich) are not marked. The surface rapidly develops an A-rich layer that is followed by a B-rich layer and these layers grow with time. In the early stages ($\tau \leqslant 30$), there is a second A-rich layer following a B-rich layer, but it breaks up in the later stages. Because of the ongoing accretion of the component A on the surface layer, the region in the vicinity of the surface is depleted in A and the domain morphology is dropletlike rather than bicontinuous, as in the bulk. This is particularly evident at later times, e.g., $\tau=9000$. Thus, in the late stages, the morphology in order of increasing Z is as follows: (a) an A-rich layer at the surface, (b) a B-rich layer, (c) A droplet (off-critical) morphology with A as the majority phase, and (d) a bicontinuous morphology associated with spinodal decomposition in the bulk.

Figure 2 shows the laterally averaged order-parameter profiles $\phi_{\rm av}(Z,\tau)$ vs Z corresponding to the evolution depicted in Fig. 1. These profiles are obtained by averaging the order parameter along the X direction for a typical run and subsequently averaging over 200 independent runs. For clarity, we only show the region with $Z \leqslant 80$. In the bulk, spinodal decomposition waves are isotropic and randomly oriented. Therefore, the averaging procedure specified above gives rise to a ''flat'' profile $\phi_{\rm av}(Z,\tau) \sim 0$. However, near the surface, this procedure gives rise to the systematic profile seen in Fig. 2 because of the anisotropic surface-directed spinodal decomposition waves [4].

It is seen that the hallmark of surface-directed spinodal decomposition, viz., a profile that oscillates with a characteristic wavelength (which is 2π in our units), is present at early and intermediate times but not at late times. In the late stages, the growing wetting layer at the surface and the subsequent depletion region replace the oscillatory structure. It is interesting to note that subsequent to the depletion region, there is another region of an enhanced order parameter with approximately the same thickness as the depletion layer. This is a consequence of coarsening in the bulk, where the system tends to minimize the interfacial energy and thus forms droplets of the A-rich phase between the B-rich layer and the bicontinuous morphology, as seen in Fig. 1.

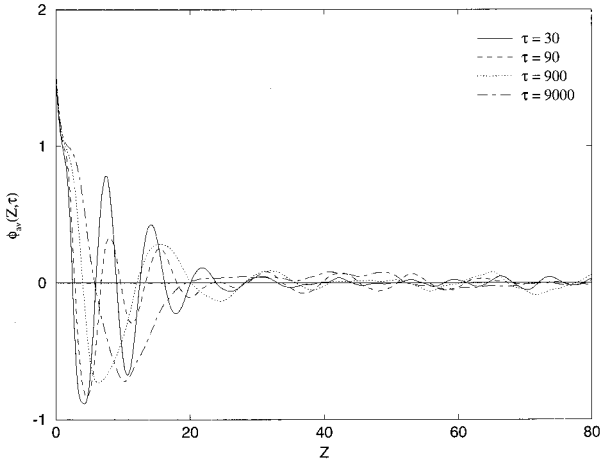

FIG. 4. Analogous to Fig. 2, but for parameter values $h_1=8$ and $n=\infty$.

Before we proceed, it would be appropriate to compare these results with our earlier results, obtained in the context of a δ-function surface potential, corresponding to $n=\infty$ in Eq. (1). Figure 3 shows evolution pictures for the case with $h_1=8$ and $n=\infty$, also corresponding to a completely wet

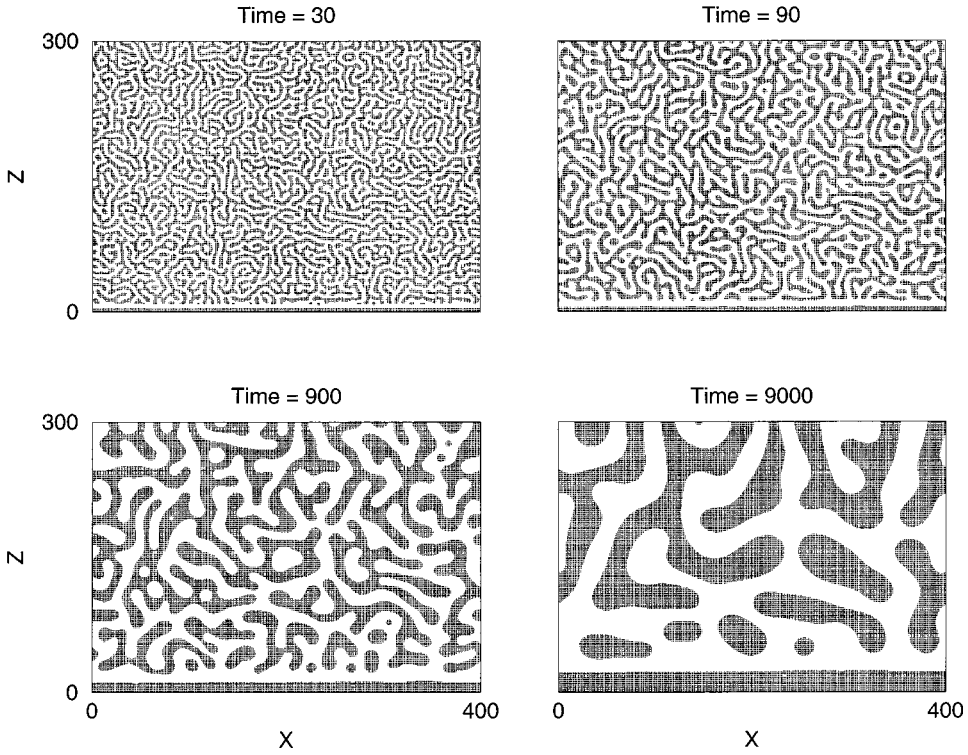

FIG. 5. Analogous to Fig. 1, but with $h_1=8$ and $n=1$. This form of the potential is somewhat unphysical, but may be possible to engineer in a suitable experiment.

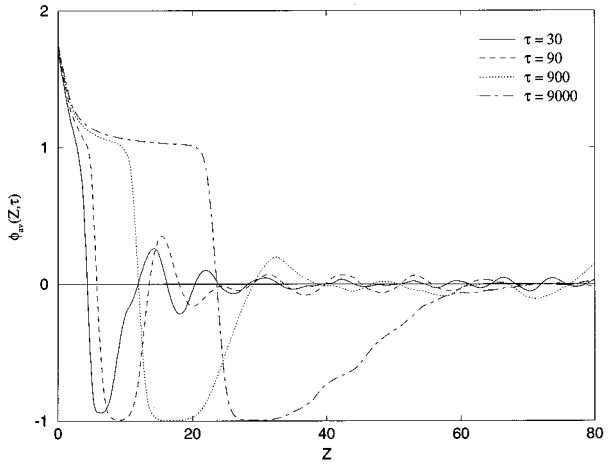

FIG. 6. Analogous to Fig. 2, but with $h_1=8$ and $n=1$.

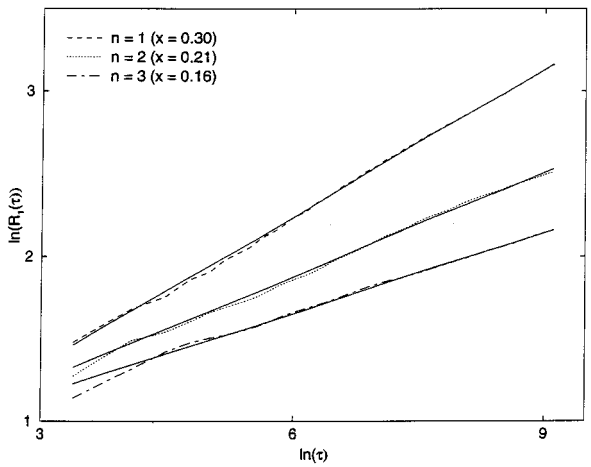

FIG. 7. Time dependence of first zero $R_1(\tau)$ of laterally averaged order-parameter profiles for surface-directed spinodal decomposition. We present data on a log-log plot for $n=1$, 2, and 3, denoted by the specified line types. The solid lines denote the best linear fits to the various data sets and the numbers specified are the corresponding best-fit exponents, denoted as x. The error bars on the exponents are ± 0.01.

static equilibrium [6]. To facilitate a comparison, we have used the same initial condition for the evolutions depicted in Figs. 1 and 3. The final frames of these figures (at $\tau=9000$) differ up to a depth of $Z\sim 70$, giving a measure of the difference between the δ-function potential and the van der Waals potential. We will quantify this difference shortly. Figure 4 shows the laterally averaged profiles corresponding to the evolution depicted in Fig. 3, plotted on the same scale as Fig. 2.

For completeness, Fig. 5 shows evolution pictures for the case $h_1=8$ and $n=1$. Of course, the interaction potential in this case is somewhat unphysical, but this example clarifies the extent to which the effect of the surface can be ''felt'' inside the bulk. Again, the initial condition for the evolution is the same as that for Figs. 1 and 3. Figure 6 shows the laterally averaged order-parameter profiles corresponding to the evolution in Fig. 5.

A quantitative measure of the temporal evolution of surface-directed spinodal decomposition waves is the first zero crossing $R_1(\tau)$ of the profiles shown in Figs. 2, 4, and 6. This quantity is also a measure of the thickness of the growing wetting layer. Figure 7 is a log-log plot of $R_1(\tau)$ vs τ for the field strength $h_1=8$ and the cases with $n=1$, 2, and 3. As observed earlier [6], the case with $n=\infty$ (not depicted here) shows barely any growth of the surface layer over the large time window considered. The data sets show a reasonable power-law behavior over the time range considered. The solid lines superposed on the data sets correspond to the best linear fits. The corresponding best-fit exponents are $x=0.30$, 0.21, and 0.16 for $n=1$, 2, and 3, respectively. The error bars on these exponent values are ± 0.01. As we will see later, these growth exponents are universal across a range of values for h_1.

At this stage, we would like to make two relevant observations. First, the dependence of the growth exponent on the nature of the surface potential is in contrast to the universality observed by other authors [7–9]. These studies considered the opposite limit of weak surface field and high interfacial tension and thermal noise, where the surface morphology is only partly wet and both A- and B-rich domains are in contact with the surface. In that case, one observes that $R_1(\tau)$ obeys the LS growth law, i.e., $R_1(\tau)\sim\tau^{1/3}$, for a variety of surface potentials. This is a possible consequence of the fact that the surface field and resultant wetting phenomena are deemphasized with respect to spinodal decomposition, so one obtains LS growth laws for all quantities. Our second observation is that Lipowsky and Huse [11] have analytically studied the growth of wetting layers in the case of stable or metastable homogeneous binary mixtures and have formulated growth laws for various dimensionalities and values of n. Their studies show that the thickness of the wetting layer $R_1(\tau)\sim\tau^x$, with $x=1/4$, 1/6, and 1/8 for $n=1$, 2, and 3, respectively. For the case with nonconserved order parameter, Lipowsky [12] predicted exponents twice as large, viz., $x=1/2$, 1/3, and 1/4 for $n=1$, 2, and 3, respectively. We emphasize that these exponents are obtained in the context of systems that are in thermal equilibrium in the bulk, whereas we consider systems that are far from equilibrium in the bulk. As regards the growth of wetting layers in unstable binary mixtures, it has been claimed by other authors that the LS growth law would characterize the growth of the wetting layer [7]. Our results demonstrate that this claim is not correct and is valid (at least numerically) only in the limit of partially wet surface morphology. Clearly, it would be relevant to formulate general analytical principles for the growth of wetting layers in phase-separating binary mixtures.

We next consider the scaling behavior of real-space correlation functions, which are useful in characterizing the dynamics of fluctuations. We define Z-dependent correlation functions parallel and perpendicular to the surface as [6]

$$G_{\parallel}(X,Z,\tau)=\langle\phi(X_1,Z,\tau)\phi(X_1+X,Z,\tau)\rangle-\langle\phi(X_1,Z,\tau)\rangle\times\langle\phi(X_1+X,Z,\tau)\rangle, \tag{5}$$

$$G_{\perp}(Z_1,Z,\tau)=\langle\phi(X,Z,\tau)\phi(X,Z+Z_1,\tau)\rangle-\langle\phi(X,Z,\tau)\rangle\times\langle\phi(X,Z+Z_1,\tau)\rangle. \tag{6}$$

In Eq. (5), the angular brackets refer to an averaging over 200 independent runs and also an integration over X_1. Similarly, in Eq. (6) the angular brackets refer to an averaging over initial conditions and an integration over X. We extract length scales from the correlation functions as the distances over which they decay to half their maximum values, which are $G_{\parallel}(0,Z,\tau)$ and $G_{\perp}(0,Z,\tau)$, respectively. The characteristic length scales in the parallel and perpendicular directions are denoted as $L_{\parallel}(Z,\tau)$ and $L_{\perp}(Z,\tau)$, respectively.

Figures 8(a)–8(c) superpose data from different times for the normalized correlation function $G_{\parallel}(X,Z,\tau)/G_{\parallel}(0,Z,\tau)$ vs $X/L_{\parallel}(Z,\tau)$ for three different values of Z. The parameter values are $h_1=8$ and $n=3$. Figure 8(a) corresponds to $Z=4$, which lies well inside the A-rich layer at the surface. In our earlier work [6], we had not considered the possibility of scaling inside the enriched layer. Figure 8(a) demonstrates that there is a reasonable scaling of the data up to $X/L_{\parallel}\sim 2$, though the tail region is still drifting. For purposes of comparison, the scaled bulk correlation function is also shown in Fig. 8(a) (as a solid line). The scaled correlation function for $Z=4$ clearly differs considerably from the bulk correlation function. This is a consequence of the strongly off-critical nature of the background at $Z=4$. As a matter of fact, a simple analysis of linear fluctuations for the one-dimensional CH equation about such a background shows that the corresponding normalized correlation function has approximately the form

$$\frac{G_{\parallel}(X,Z,\tau)}{G_{\parallel}(0,Z,\tau)} \simeq \left(1-\frac{X^2}{4\alpha\tau}\right)\exp\left(-\frac{X^2}{8\alpha\tau}\right), \tag{7}$$

where $\alpha=3\phi_0(Z)^2-1$, with $\phi_0(Z)$ being the background value from the equilibrium profile. The above form is valid in the region where local equilibrium has been established and where $\phi_0(Z)$ is large and does not vary rapidly with Z. The length scale associated with these fluctuations is $L_{\parallel}(Z,\tau)\sim\tau^{1/2}$.

Figures 8(b) and 8(c) clarify the dynamical evolution of the scaled correlation function more clearly. In Fig. 8(b), which corresponds to $Z=20$, the scaled correlation function for $\tau=840$ is closest to the bulk form and evolves in time towards a form corresponding to an off-critical morphology, as the wetting layer penetrates deeper into the bulk. The same trend is seen in Fig. 8(c), which corresponds to $Z=24$. There is a sharp contrast between these results and our earlier results for the δ-function potential [6] in that we can clearly observe the dynamical effects of growth of the wetting layer in the present case.

To stress this point further, Fig. 9(a) plots $L_{\parallel}(Z,\tau)$ vs τ for $Z=20,24,28$ and the bulk. We do not present results for $Z<20$ because the data are too ragged to discern any systematic trend, in spite of the reasonable scaling for $Z<20$. The length-scale data for different values of Z follow the bulk behavior initially and then cross over to a faster growth as the effect of the wetting layer is felt. The crossover is later for larger values of Z and the results in this figure should be correlated with the inward propagation of profiles in Fig. 2. Figure 9(b) plots the data of Fig. 9(a) on a log-log scale and clarifies the crossover behavior. Subsequent to the crossover, the accelerated growth seems to fit a faster growth law $L_{\parallel}(Z,\tau)\sim\tau^{1/2}$, though we do not have sufficiently extended

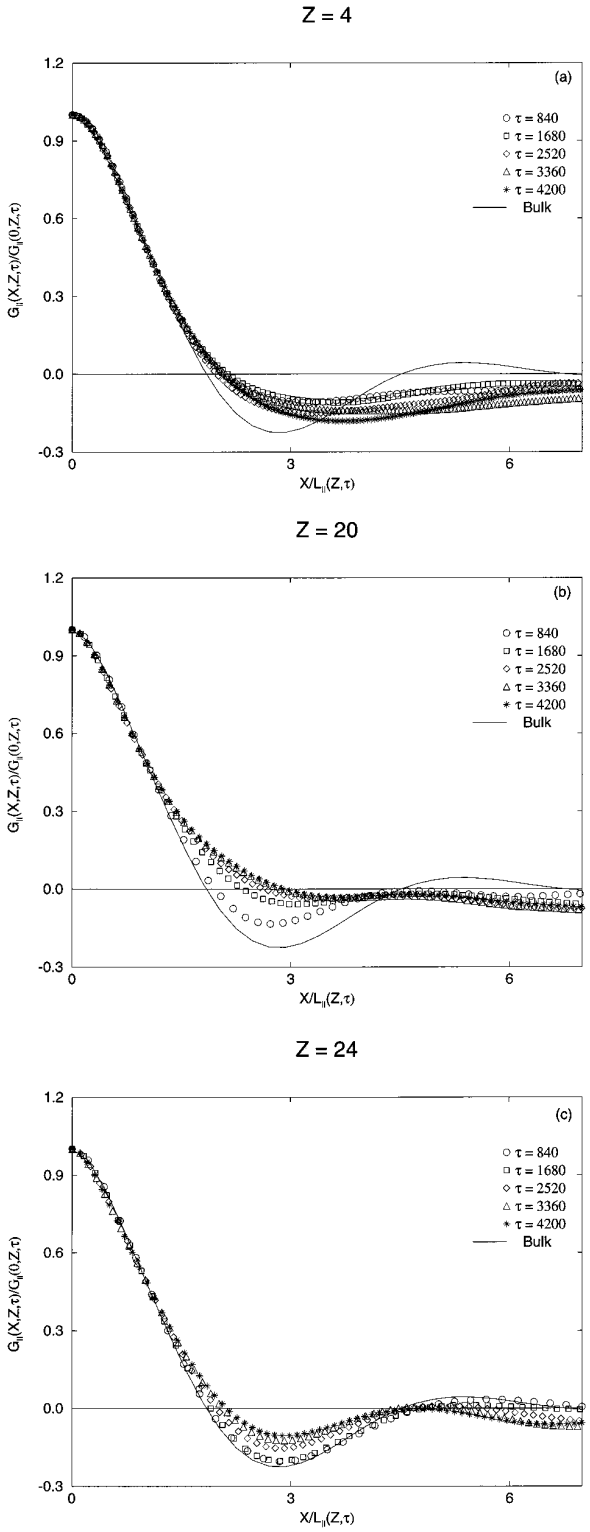

FIG. 8. Scaled plots of depth-dependent real-space correlation functions in the direction parallel to the surface. The correlation functions are obtained as described in the text. We superpose scaled data for $G_{\parallel}(X,Z,\tau)/G_{\parallel}(0,Z,\tau)$ vs $X/L_{\parallel}(Z,\tau)$ from dimensionless times 840, 1680, 2520, 3360, and 4200, denoted by the specified symbols. The length scale $L_{\parallel}(Z,\tau)$ is defined as the distance over which the correlation function decays to half its maximum value. For purposes of comparison, we also present the scaled bulk correlation function as a solid line. Data are presented for (a) $Z=4$, (b) $Z=20$, and (c) $Z=24$.

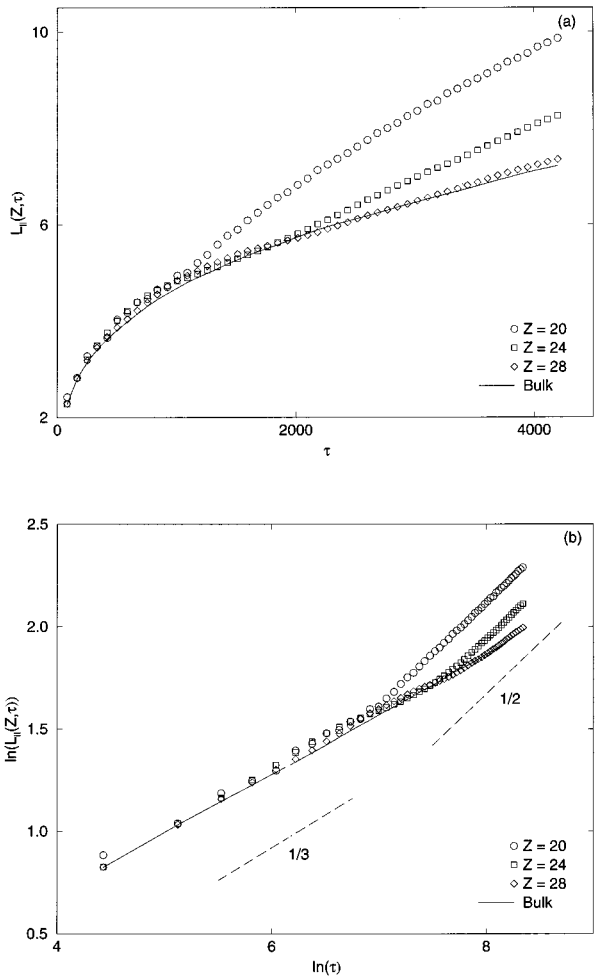

FIG. 9. (a) Time dependence of the length scale in the direction parallel to the surface, viz., $L_\parallel(Z,\tau)$ vs τ. We present data for $Z=20$, 24, and 28, denoted by the specified symbols. Data for the bulk length scale are denoted by the solid line. (b) A log-log plot of the data in (a). The dashed lines have slopes 1/3 and 1/2, respectively.

data to make a conclusive statement in this context. As we had pointed out earlier, fluctuations about a highly off-critical background exhibit a growth law $\sim\tau^{1/2}$. However, we should emphasize that the background profile at the values of Z considered in Fig. 9 is not strongly off critical at the time of crossover (see Fig. 2). Thus the data in the crossover regime may be associated with the orientational effect of the layered structure at the surface. In that case, the data should exhibit the LS growth law, but with a larger prefactor than in the bulk. The deceptively larger exponent in Fig. 9(b) is a possible consequence of attempting to fit crossover data to a power-law form.

It is also possible that the $L_\parallel(Z,\tau)\sim\tau^{1/2}$ behavior is a transient regime, caused by the breakup of the bicontinuous morphology into elongated droplets, oriented parallel to the wall on the average. These droplets have a strong tendency to compactify subsequently. It is possible that this mechanism leads to a transient regime of faster growth before the isolated droplets disappear again to ''feed'' the growing wetting layer and the subsequent depletion layer, while new isolated droplets form farther inside somewhat later, etc.

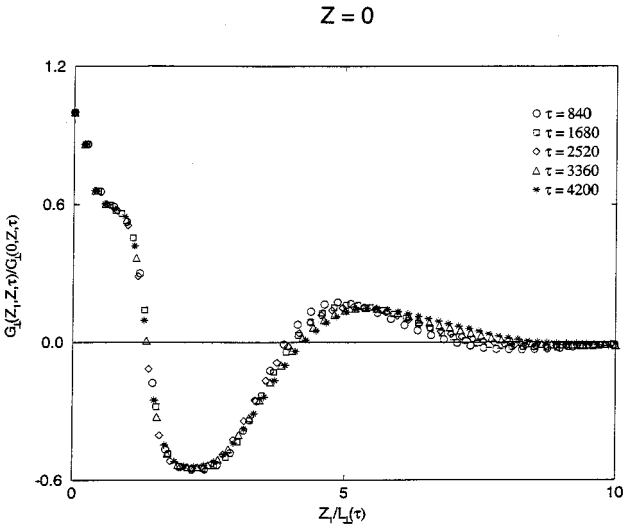

FIG. 10. Superposition of data for the normalized correlation function in the perpendicular direction, i.e., $G_\perp(Z_1,Z,\tau)/G_\perp(0,Z,\tau)$ vs $Z_1/L_\perp(Z,\tau)$. We present data for $Z=0$ and dimensionless times $\tau=840$, 1680, 2520, 3360, and 4200, denoted by the specified symbols.

We next consider the dynamical behavior in the direction perpendicular to the surface. Figure 10 plots the normalized correlation function $G_\perp(Z_1,Z,\tau)/G_\perp(0,Z,\tau)$ at $Z=0$ vs $Z_1/L_\perp(\tau)$ for dimensionless times $\tau=840$, 1680, 2520, 3360, and 4200. The correlation function exhibits reasonable scaling and clearly follows the functional form of the laterally averaged profiles in Fig. 2. This plot suggests that the thickness of the growing wetting layer and that of the subsequent depletion layer are always of the same order of magnitude. Figure 11(a) plots $L_\perp(Z,\tau)$ vs τ for $Z=20,24,28$ and the bulk and should be correlated with Fig. 9(a). Figure 11(b) is a plot of Fig. 11(a) on a log-log scale. The picture that emerges is that both the perpendicular and parallel length scales follow the LS growth law until they experience the effect of the wetting layer. At that stage, the parallel length scale shows accelerated growth, whereas the perpendicular length scale exhibits decelerated growth and can even freeze. This ''freezing'' does not mean that there is no temporal evolution; rather, the point Z ''leaves'' the region of bicontinuous morphology and becomes part of the droplet region and later the depletion region, whereas $Z+Z_1$ still lies in the region of bicontinuous morphology. This change in character of the correlation offsets the growth seen in the corresponding profiles in Fig. 2. This strong interplay of wetting and phase separation was not seen in our simulations for the δ-function potential, where the wetting layer moved too slowly to have any discernible impact on spinodal decomposition [6]. In the δ-function case, we only observed the orientational effects of the ordered structure at the surface.

We have also obtained similar results for the cases with $h_1=8$ and $n=1,2$. Essentially, the main features are the same as above, but all effects are more marked. In the interest of brevity, we do not present these results here. We have also obtained detailed results for other values of h_1. For completeness, we will present some representative results for different values of h_1 here. Figure 12 compares evolution

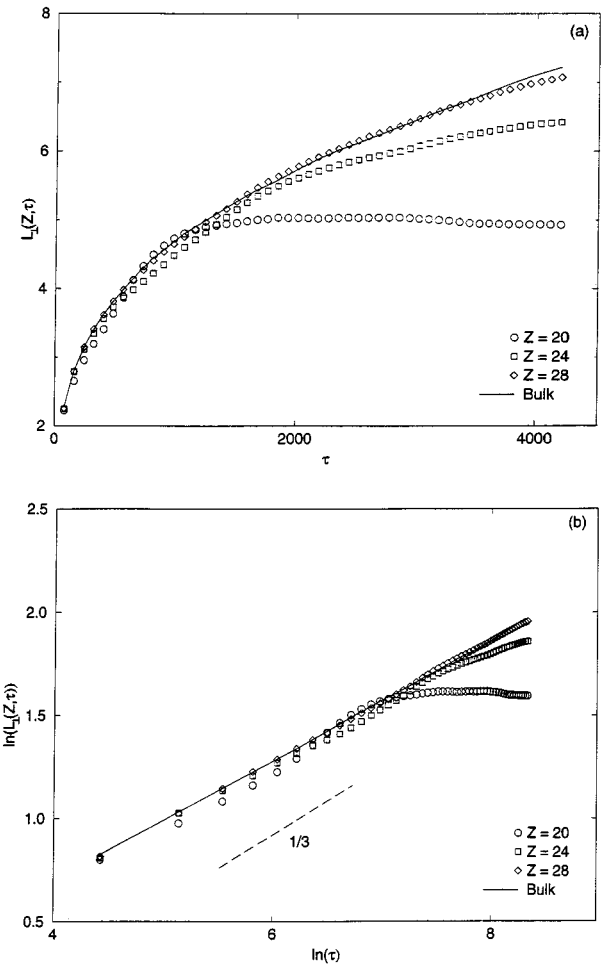

FIG. 11. (a) Analogous to Fig. 9(a), but for the perpendicular length scale $L_\perp(Z,\tau)$. (b) A log-log plot of data in (a). The dashed line has a slope of 1/3.

pictures for the cases with $h_1=2$ and $n=3,\infty$. (To facilitate a comparison with previous evolution pictures in Figs. 1, 3, and 5, we always use the same initial condition.) Results for $n=\infty$ are shown in the two upper frames (corresponding to $\tau=900$ and 9000) and it is clear that these parameter values correspond to a partially wet morphology [6], with both A- and B-rich domains in contact with the surface. Results for the case $n=3$ are shown in the two lower frames and correspond to a plated or layered morphology. Figure 13 is a log-log plot of $R_1(\tau)$ vs τ for laterally averaged profiles in the cases with $h_1=2$ and $n=1,\ 2,\ 3$, and ∞. The data for the cases with $n=1,\ 2$, and 3 again exhibit a reasonable power-law behavior and the growth exponents are compatible with those for $h_1=8$ (see Fig. 7). However, in the case with $n=\infty$, the growth of $R_1(\tau)$ is appreciably larger than before, though not systematic enough to be properly characterized. This behavior should be compared with earlier results for the growth of surface ''layers'' in the case with partially wet morphology [8,9].

Finally, we mention results for the case $h_1=12$ and $n=1,\ 2,\ 3$, and ∞. Again, the thickness of the wetting layer exhibits a power-law behavior with best-fit exponents $x=0.31,\ 0.21$, and 0.16 for $n=1,\ 2$, and 3, respectively. These exponents are in agreement with those in Figs. 7 and 13. Furthermore, results for the $n=\infty$ case are similar to those for $h_1=8$ and do not exhibit a power-law behavior.

IV. SUMMARY AND DISCUSSION

Let us end this paper with a summary and discussion of our results. In previous work [6], we have presented a model [and detailed numerical results for surface-directed spinodal decomposition with a short-ranged surface potential. In Ref.

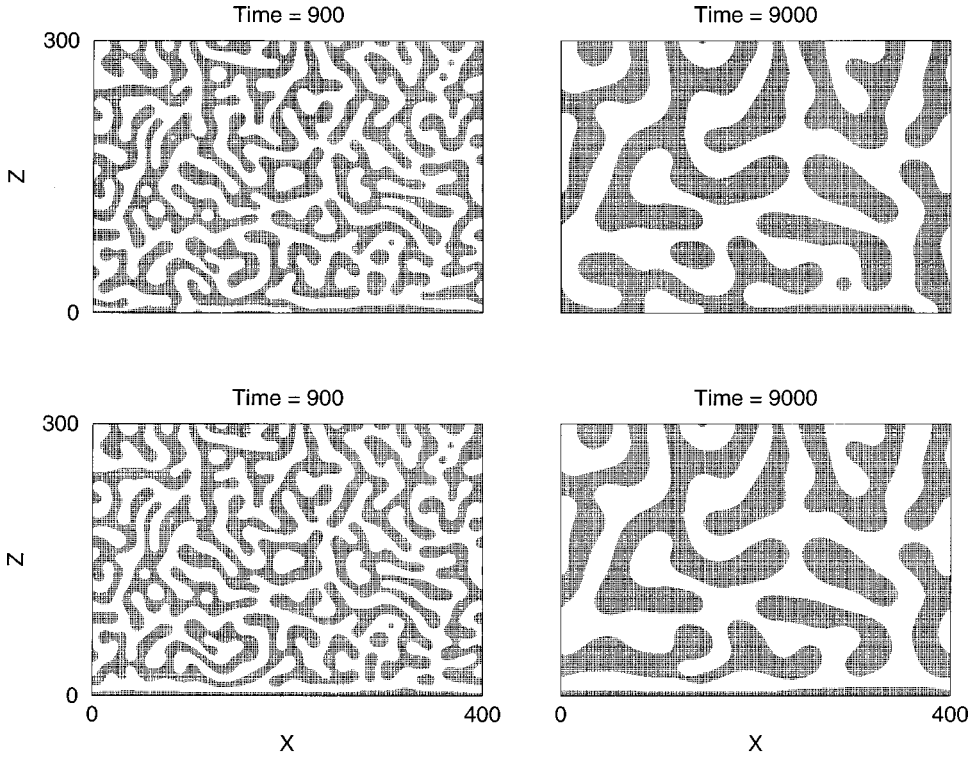

FIG. 12. Evolution pictures similar to those shown in Fig. 1, but for the field strength $h_1=2$. The two upper frames correspond to $n=\infty$ (δ-function potential) and the two lower frames correspond to $n=3$. All other parameter values and simulation details are the same as in Fig. 1.

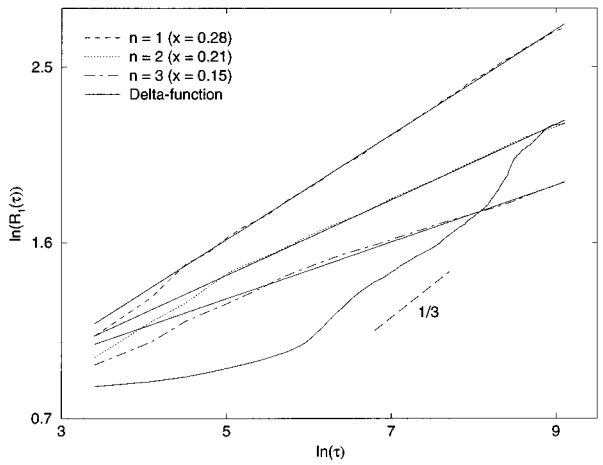

FIG. 13. Analogous to Fig. 7, but for the field strength $h_1=2$. Furthermore, in this case, we also present data for the case $n=\infty$, corresponding to a δ-function surface potential. The dashed line has a slope of 1/3. Again, the error bars on the specified exponents x are ± 0.01.

6 we also formulated tools for the proper characterization of domain growth in the presence of a surface. The present paper is an extension of our previous work to the case of a surface that exerts long-ranged forces on the preferred component of a binary mixture. In particular, the present work is more relevant to experimental situations, where the surface usually interacts with molecules of the binary mixture via long-ranged van der Waals interactions. Our model in this paper is a simple extension of our earlier model for the case with a δ-function potential [6] and we use similar tools to characterize domain growth. However, we obtain a number of different results that we would like to highlight below.

Our first relevant observation is that the thickness of the wetting layer, measured by the first zero $R_1(\tau)$ of the laterally averaged order-parameter profiles, exhibits a power-law growth for potentials as in Eq. (1) with $n=1$, 2, and 3. The growth exponents are universal across a range of values of field strength h_1, but depend sensitively on the value of n. For the short-ranged case ($n=\infty$), the growth of the wetting layer does not obey a power law. It appears to be logarithmic, but we do not have sufficient data to ascertain this conclusively. These results are at variance with the claim [7] that the wetting layer always exhibits LS growth when the binary mixture in the bulk is undergoing spinodal decomposition. We believe that this claim is valid only in the limit of a partially wet surface morphology, with domains rich in both phases being in contact with the surface. These results of ours should be verifiable experimentally. Furthermore, we also hope that our numerical results will facilitate a generalization of the analytic treatment of Lipowsky and Huse [11], who considered the growth of wetting layers in stable or metastable homogeneous binary mixtures.

The second observation is that our present results clearly enable us to see the interplay between wetting and spinodal decomposition. In our previous work [6], the growth of the wetting layer was so slow that it was not possible to see the dynamical effect of the wetting layer on phase separation. In our present work, we can follow the emergent anisotropy of domain growth as the surface-directed spinodal decomposition waves penetrate into the bulk. In particular, we can track the evolution of the depth-dependent correlation function parallel to the surface from the ''bulk'' form at early times to a form corresponding to an off-critical morphology at late times. Simultaneously, we also observe the acceleration and deceleration of length scales parallel and perpendicular to the surface, respectively.

Finally, in the present study, we have also examined the scaling of fluctuations deep inside the wetting layer at the surface. It is somewhat surprising that the correlation function parallel to the surface inside the layer exhibits reasonable scaling even though the associated length scales show fairly erratic behavior numerically.

The problem of surface-directed spinodal decomposition has evolved as the result of a close interaction between experimental studies and numerical simulations. We hope that the present set of numerical results will also prove amenable to experimental investigation.

ACKNOWLEDGMENTS

S.P. would like to thank R.A.L. Jones and J. Marko for useful discussions. He would also like to thank K. Binder for his kind hospitality in Mainz, where this work was completed. S.P.'s stay in Mainz was supported by the Deutsche Forschungsgemeinschaft under Sonderforschungsbereich 262. H.L.F.'s stay in Mainz was supported by the Humboldt Foundation. He was also partly supported by NSF Grant No. DMR 962-8224.

[1] For a review of modeling and numerical simulations of this problem see S. Puri and H.L. Frisch, J. Phys.: Condens. Matter **9**, 2109 (1997).

[2] For a review of experimental techniques and results for this problem, see G. Krausch, Mater. Sci. Eng. Rep. **14**, 1 (1995).

[3] For reviews of phase separation kinetics in the bulk see J.D. Gunton, M. San Miguel, and P.S. Sahni, in *Phase Transitions and Critical Phenomena*, edited by C. Domb and J.L. Lebowitz (Academic, New York, 1983), Vol. 8, p. 267; K. Binder, in *Materials Science and Technology, Vol. 5: Phase Transformations of Materials*, edited by R.W. Cahn, P. Haasen, and E.J. Kramer (VCH, Weinheim, 1991), p. 405.

[4] R.A.L. Jones, L.J. Norton, E.J. Kramer, F.S. Bates, and P. Wiltzius, Phys. Rev. Lett. **66**, 1326 (1991).

[5] K. Binder and H.L. Frisch, Z. Phys. B **84**, 403 (1991).

[6] S. Puri and K. Binder, Phys. Rev. A **46**, R4487 (1992); Phys. Rev. E **49**, 5359 (1994).

[7] Z. Jiang and C. Ebner, Phys. Rev. B **39**, 2501 (1989).

[8] G. Brown and A. Chakrabarti, Phys. Rev. A **46**, 4829 (1992).
[9] J.F. Marko, Phys. Rev. E **48**, 2861 (1993).
[10] Y. Oono and S. Puri, Phys. Rev. Lett. **58**, 836 (1987); Phys. Rev. A **38**, 434 (1988); S. Puri and Y. Oono, *ibid.* **38**, 1542 (1988); J. Phys. A **21**, L755 (1988); T.M. Rogers, K.R. Elder, and R.C. Desai, Phys. Rev. B **37**, 9638 (1988); A. Chakrabarti and J.D. Gunton, *ibid.* **37**, 3798 (1988).
[11] R. Lipowsky and D.A. Huse, Phys. Rev. Lett. **37**, 353 (1986).
[12] R. Lipowsky, J. Phys. A **18**, L585 (1985).